J. Fluid Mech. (2004), *vol.* 513, *pp.* 47–75.
DOI: 10.1017/S0022112004009723 Printed in the United Kingdom

Symmetry breaking, ring formation and other phase boundary structures in shock tube experiments on retrograde fluids

By HAITAO FAN

Department of Mathematics, Georgetown University, Washington, DC 20057, USA
fan@math.georgetown.edu

(Received 15 March 2002 and in revised form 18 February 2004)

A peculiar multi-dimensional wave pattern in shock tube experiments on retrograde fluids is the ring formation phenomenon. When the incident shock is reflected by the endwall of a shock tube filled with retrograde fluid vapour, under certain conditions, rings of liquid/vapour mixture form behind the reflected shock. In this paper, we find the reason for such symmetry breaking and ring formation phenomena by studying a prototype model for flows with liquid/vapour phase transitions. The isothermal case of this model exhibits all major one-dimensional wave patterns observed in shock tube experiments on retrograde fluids. The symmetry is broken by the liquid or liquid/vapour drops initiated behind the reflected shock where the pressure is higher than the equilibrium pressure. Liquid drops become liquid/vapour mixture drops later. Using a liquid/vapour mixture drop at the reflecting wall as the initial condition for the prototype model, it is shown that this drop will evolve into a ring, yielding the explanation for ring formation. The outer fronts of rings are collapsing waves. Such waves are supersonic, as confirmed by some photographs of actual experiments. It is also shown that a liquid or liquid/vapour mixture drop cannot evolve into a ring if no reflecting wall is present, agreeing with experimental observation. A mechanism is also provided by the model for the emergence of the 'button' at the centre of, and the small-scale asperities at, the liquefaction shock front observed at the exit of the open-end shock tube.

1. Introduction

Liquid/vapour phase transitions have been studied for decades. However, many issues are still open. For example, Dettleff *et al.* (1979) found in their shock tube experiments on retrograde fluids that rings of liquid/vapour mixture would form randomly behind reflected shocks. Although several attempts have been made to identify the reason for the ring formation, the phenonmena still remains to be explained. In this paper, we shall present an explanation for ring formation through analysis of waves in the prototype model proposed and developed in Fan (1998, 2000*b*) for qualitative investigation of liquid/vapour phase transitions in shock tubes. We shall further explain the small-scale surface structures of liquefaction shocks observed in experiments.

Basic observations on fluids exhibiting liquid/vapour phase transitions involving metastability are as follows: The pressure functions $p(\rho, T)$ for such fluids have the shape depicted in figure 1 when T is fixed. Here ρ is the density and T the temperature. The region $\rho < \alpha$ corresponds to vapour, while $\rho > \beta$ corresponds to liquid. The line

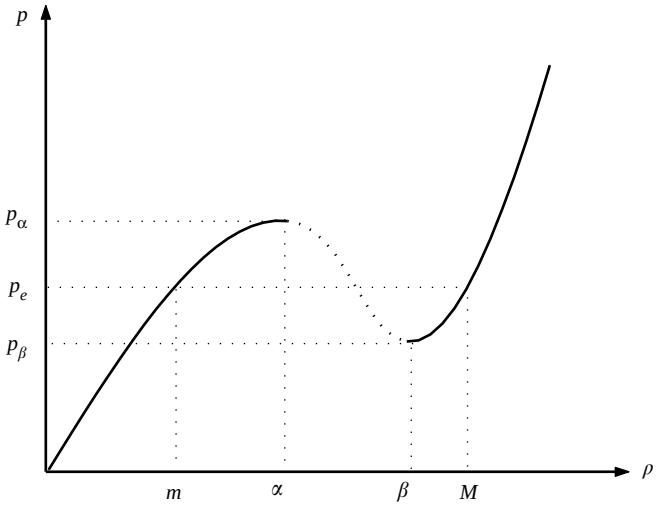

FIGURE 1. The pressure function $p(\rho, T)$ for fixed T.

joining $(m, p(m, T))$ and $(M, p(M, T))$ is called the Maxwell line, where liquid and vapour can coexist in equilibrium. The spinodal region $\rho \in [\alpha, \beta]$ is a highly unstable region where the fluid, if it can enter, will quickly decompose into vapour or liquid or their mixture. Thus, the pressure curve $p(\rho, T)$ in this region cannot, at present, be measured. The metastable region $m < \rho < \alpha$ (or $\beta < \rho < M$) is where pure vapour (or liquid) can stay for some time with little condensation (or evaporation) until enough liquid (or vapour) nuclei are initiated.

Research on fluid flows involving liquid/vapour phase transitions has been very active since the groundbreaking work of Oswatitsch (1942). It includes many challenging areas of research such as state functions of fluids, multi-phase flows in various fluid configurations, nucleation and droplet growth rates, to name just a few. The literature in this area is too large to cite here. The reader is referred to re-break view articles such as Wegener (1969, 1975), Wegener & Mack (1958), Wegener & Wu (1977), Kotake & Glass (1981), for flows with condensation, and Abraham (1974), Fuchs & Sutugin (1970), Oxtoby (1992), Springer (1978), Wagner (1982), for nucleation and droplet growth rates; and references cited therein. Flows involving evaporation are typically more complicated, see Skripov (1974) for more information. Most previous works are about phase transition flows in shock tubes, condensation in supersonic nozzles and other expansion/compression devices. Since this paper is closely related to phase transition flows in shock tubes, we only mention Kotake & Glass (1981), Delale, Schnerr & Zierep (1993*a*, *b*) as a starting point for references on flows in other devices such as nozzles. Studies on condensation in expansion waves in shock tubes, using regular fluids with inert carrier gases, were initiated and developed by Wegener & Lee (1983), Wegener & Lundquist (1951), Wegener & Wu (1977). Many authors have contributed to the study of flows with phase transitions in shock tubes, such as Bauschdorff (1975), Glass, Kalra & Sisilian (1977), Homer & Hurle (1972), Kotake & Glass (1977), Kawada & Mori (1973), Lee (1978), Sisilian (1975), Sisilian & Glass (1976), and Wu (1977). Dettleff *et al.* (1979), Gulen, Thompson & Cho (1994), Thompson, Carofano & Kim (1986), and Thompson *et al.* (1987) carried out experimental and computational studies on phase transitions in shock tubes using

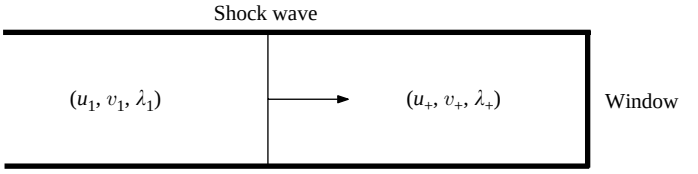

FIGURE 2. A compression shock is sent into stable vapour at rest. Here, $\lambda_1 = \lambda_+ = 1$, $\boldsymbol{u}_1 = u_1\boldsymbol{k}$ with $u_1 < 0$ and $\boldsymbol{k}$ denoting the direction along the centre axis of the shock tube away from the end window.

retrograde fluids (i.e. fluids with large heat capacity), where they observed a number of interesting wave patterns. There are some studies on the flows of retrograde fluids in supersonic nozzles, see Kluwick & Scheichl (1996) and references cited therein.

The behaviour of regular fluids and retrograde fluids can be quite different in adiabatic experiments. For example, consider the vapour at equilibrium pressure in an adiabatic container. When compressed, the pressure of the fluid p will increase, so will the temperature T and the equilibrium pressure $p_e(T)$. Given the same increase in pressure, the temperature of a regular fluid increases more than that of a retrograde fluid since the latter has higher heat capacity. Thus, the equilibrium pressure $p_e(T)$ of a regular fluid increases more than that of a retrograde fluid. The heat capacity of a retrograde fluid is large enough so that the pressure after compression p is higher than $p_e(T)$, resulting in condensation. For a regular fluid, the pressure after compression p is lower than $p_e(T)$, and hence condensation will not occur. When a container of the fluid is in a heat bath to keep the temperature constant, and heat conduction is rapid, then the above mechanism is absent and the regular fluid will behave like a retrograde fluid.

For definiteness, in this paper, we shall concentrate on retrograde fluids or fluids in the isothermal case. Experimental observations for such fluids can be compared with analytical results for isothermal models.

Dettleff *et al.* (1979) and Thompson *et al.* (1986, 1987) summarized the major wave patterns involving phase transitions observed in shock tube experiments on retrograde fluids. Their experimental apparatus was a tube with a piston (or a substitute) on one side, say the left side, with the other side either open or closed. Compressing or withdrawing the piston can induce phase transition. The following is a list of these wave patterns:

(*a*) Ring formation. This is a particular multi-dimensional wave pattern related to phase changes. In this case, a glass window closes one end of the shock tube. The tube is filled with stable vapour. A dry shock, i.e. a shock in vapour without phase transition, is sent into the tube (see figure 2). The shock is chosen so that the pressure behind it is still below the equilibrium pressure. After the shock is reflected by the glass window, the pressure behind the reflected shock is higher than the equilibrium pressure, resulting in condensation. Dettleff *et al.* (1979) observed that the condensation occurs in two stages. At first, rings of liquid/vapour mixture are observed just behind the reflected shock at the window, as shown in figure 3. Then these rings quickly spread out to complete condensation behind the reflected shock. Such rings were not observed in experiments with open-end shock tubes, even when the Mach number of the liquefaction shock was high, Kim (1987), Thompson *et al.* (1987).

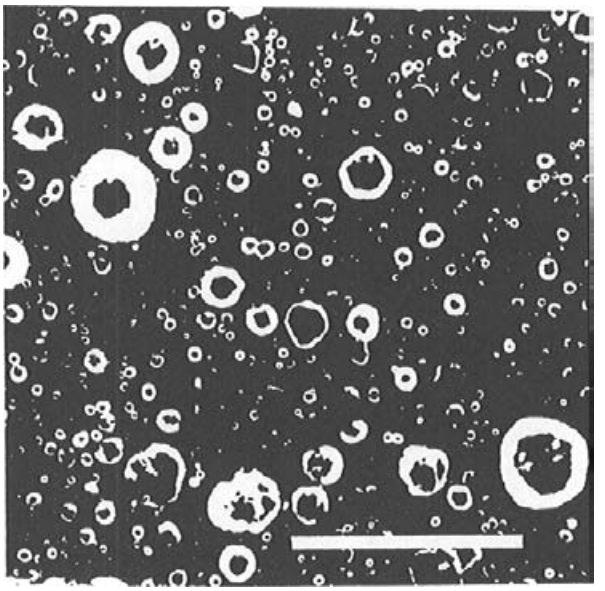

FIGURE 3. Rings of liquid/vapour mixture appear at the window and behind the reflected shock, Dettelff *et al.* (1979).

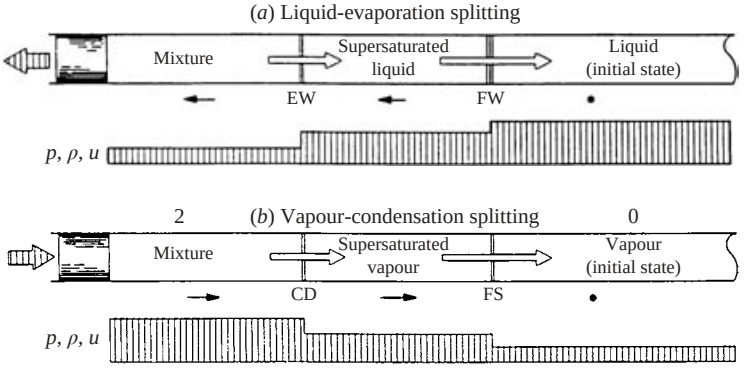

FIGURE 4. Conceptual representation of one-dimensional wave splitting in a liquid–vapour system by Thompson *et al.* (1987). All waves travel to the right. The motion of the piston is shown by the wide hatched arrows, fluid motion by thin arrows and wave motion by open arrows. (*a*) Withdrawing the piston: FW = forerunner rarefaction wave; EW = evaporation wave. (*b*) Compressing the piston: CD = condensation discontinuity; FS = forerunner dry shock.

(*b*) Rarefaction wave splitting. A rarefaction wave is sent into the liquid by withdrawing the piston from liquid. This wave then splits into a forerunner rarefaction wave, which sends the liquid into the metastable region, followed by a slower moving evaporation shock, as shown in figure 4(*a*). The upstream state of the evaporation shock is overheated liquid.

(*c*) Shock wave splitting. A shock is sent into vapour by compressing the piston into the vapour. If the shock is not too strong, it will split into a forerunner shock and a slower moving condensation discontinuity across which vapour changes to

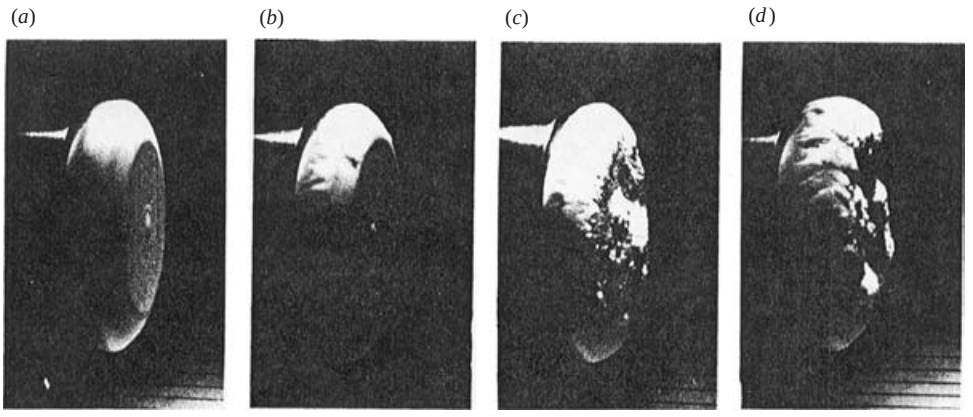

FIGURE 5. Transition from smooth to chaotic liquefaction shock fronts with increasing shock Mach number, taken from figure 20 of Thompson *et al.* (1986).

liquid/vapour mixture or liquid, as shown in figure 4(*b*). On further increasing the shock strength, the condensation discontinuity will move faster, and eventually the condensation discontinuity and the forerunner shock merge if the compression is strong enough. When the upstream is equilibrium liquid/vapour mixture, then there is no wave splitting.

(*d*) Rarefaction shock. By withdrawing the piston from an equilibrium liquid/vapour mixture, a rarefaction shock is generated. The fluid downstream of the shock is overheated vapour. Pushing the piston into the equilibrium liquid/vapour mixture will create a condensation discontinuity.

(*e*) Surface structures and the transition from smooth to chaotic liquefaction shock fronts with increasing shock Mach number. As the Mach number of the incident shock increases, a variety of features appear on the surface of the liquefaction shock front. They include, in approximate order of increasing shock Mach number, a small protuberance or 'button' at the centre of the shock front (figure 5*a*); regular surface waves; small-scale surface asperities or eruptions; surface discontinuities; chaotic shock fronts.

Several attempts have been made to explain the ring formation phenomenon. When Dettleff *et al.* (1979) discovered ring formation, they guessed that these were vortex rings, and that these vortices were due to the action of the shock pressure gradient upon a liquid droplet. When the incident shock passes a liquid drop or a heavy particle of impurities, the drop accelerates slower than the surrounding vapour, causing a gradient of velocity. The difference in velocity will produce vortex rings, and the rings of mixture observed are these vortex rings. There is no detailed analysis available to justify this conjecture. According to this explanation, ring formation would occur behind any liquefaction shock if the Mach number were large enough. However, Thompson *et al.* (1987) and Kim (1987) later discovered that this is not the case: ring formation was observed consistently only when shocks were reflected by the endwall, and the reflected shock's Mach number was above 2.5. In the open-end shock tube experiments rings were absent even if the Mach number of the incident shock was above 3 (see Gulen 1992, p. 181). This suggests that the ring formation has nothing to do with fluid vortices, nor shock strength. Some photographs published in Gulen *et al.* (1994) showed that some rings expanded in the direction vertical to the incident shock at a Mach number 4 when the incident shock was of Mach

number 2.87. One ring grew to 4.1 mm in radius in less than 6 μs. There is no detailed justification available for how a tiny droplet of a few μm in radius can cause a vortex ring of a few mm in radius whose outer front travels much faster than the incident shock. Gulen (1992, p. 189) observed that in the shock reflection experiments, "with a few exceptions", the final equilibrium state behind the reflected shock was beyond the vapour spinodal limit. Thus, he conjectured that ring formation occurred because the vapour was pushed into the spinodal region. However, this explanation cannot explain (i) why the geometric structure is a ring, (ii) why compression shocks in the open-end shock tube experiments cannot push the vapour into the spinodal region even at a much higher Mach number, and (iii) why rings were also present in those 'few exceptions'.

To obtain a deeper understanding of liquid/vapour phase changes, in particular to explain ring formation and other surface structures, mathematical models have to be used. We would like to have a model that is simple enough to allow mathematical analysis but still preserves wave patterns observed in experiments in the isothermal case. Then, through the analysis of the model for evolution process of the ring formation, we can get insight into the reason for ring formation. It is even better if it is possible to make the model quantitatively accurate by using realistic state functions, parameters, or by introducing more variables and equations if necessary.

Earlier works on flows involving phase changes in shock tubes considered models similar to reactive flow equations with some complicated droplet nucleation and growth rate functions that govern the phase changes. See the review article by Kotake & Glass (1981) and references cited therein for more information. Some computations and analysis of these models for regular fluids with inert carrier gases have been carried out by Glass *et al.* (1977), Kotake & Glass (1977), Sisilian & Glass (1976), Smolders, Niessen & van Dongen (1992) and Sisilian (1975) to yield many interesting results. Whether these models can exhibit wave patterns (*a–d*) for retrograde fluids is not clear yet. These models are difficult to analyse mathematically due to the complicated droplet nucleation and growth rates. Using these models to find a clear explanation for ring formation through mathematical analysis may be difficult.

Rabie, Fowles & Fickett (1979) studied a simple model of the dynamics of phase transitions

$$\left.\begin{aligned} &\dot{\rho} + \rho u_x = 0, \quad \rho\dot{u} + p_x = 0, \quad \dot{e} + \sigma\dot{v} = 0, \\ &\dot{\lambda} = -\frac{\lambda - \lambda_e}{\gamma}\chi(p \geqslant p_{ig}), \end{aligned}\right\} \tag{1.1a}$$

where the overdot denotes the usual Lagrangian derivative along a particle path, ρ is the density, u the particle velocity, σ the stress, $v = 1/\rho$, λ the reacted mass fraction, e the specific internal energy, γ the typical reaction time and χ the characteristic function. The equilibrium reacted mass fraction is

$$\lambda_e = \begin{cases} 0 & \text{if } \rho > M, \\ \dfrac{\rho - m}{M - m} & \text{if } M \geqslant \rho \geqslant m, \\ 1 & \text{if } \rho < m, \end{cases} \tag{1.1b}$$

and p_{ig} the artificial ignition pressure. The equilibrium pressure is assumed to be constant, and hence the fluid is similar to a retrograde fluid. The term $\chi(p \geqslant p_{ig})$ is a technical assumption to make travelling waves possible. Rabie *et al.* (1979) studied the phase plane for the travelling wave equations of (1.1). They also studied the piston

problem with initial values in the metastable liquid region. They found double wave structures in the solutions. The advantage of this model is that it is simple enough to allow mathematical analysis yet still provide valuable insights. However, the choice of the reaction rate equation (1.1*b*) forces the fluid to go to equilibrium exponentially fast, which excludes the creation of metastable states. Thus, the rate law (1.1*b*) cannot be used to investigate ring formation and other phenomena associated with metastability.

The book by Fickett & Davis (1979) contains an extensive investigation of a prototype system

$$\rho_t + p(\rho, \lambda)_x = \epsilon\rho_{xx}, \quad \lambda_t = \frac{\lambda_e - \lambda}{\gamma}, \tag{1.2}$$

where λ_e is given in (1.1*b*) and $p(\rho, \lambda) = (\rho^2 + q\lambda)/2$, and $q > 0$ is a constant. Although (1.2) is a much simplified system, it captures some features of waves of detonation type in flows involving phase transitions.

Dynamic flows involving liquid/vapour phase transitions have also been studied through the investigation of the system of conservation laws

$$v_t - u_x = 0, \quad u_t + p(v)_x = 0, \tag{1.3}$$

with van der Waals types of pressure functions. When the van der Waals type of pressure function is used, the system (1.3) is of hyperbolic–elliptic mixed type. This system can reproduce wave patterns (*b*, *c*), as shown by Slemrod (1983), Shearer (1986) and Fan (1993). However, this system does not naturally allow liquid/vapour mixtures. Moreover, it cannot include some types of phase boundaries that turn out to be critical to our explanation of ring formation.

The above-mentioned models for phase transition flows are either too complicated to yield a clear explanation without a lot of technicalities or too simple to capture the ring formation phenomenon. Recently, Fan (1998, 2000*b*) proposed a model for qualitative investigation of flows involving liquid/vapour phase transitions in shock tubes. The model exhibits all the one-dimensional wave patterns (*b–d*) listed above. Here we like to point out that once the wave pattern observed in the model and in experiments match, then quantitative accuracy is possible. For example, if both the experiment and the model with the same initial data exhibit the same two-shock wave pattern as in figure 4(*b*), then the states of the fluid on both sides of the shocks are determined by the Rankine–Hugoniot conditions. The Rankine–Hugoniot conditions are algebraic equations depending only on the state functions, such as the pressure function. Therefore, quantitative accuracy is possible to achieve with more accurate state functions and parameters once the wave patterns match. Fan (2000*a*) showed that the nucleation rate term in the model, in the context of figure 4(*b*), accelerates the slower moving condensation discontinuity up to the speed of the forerunner dry shock. The larger the nucleation rate, the faster the condensation discontinuity moves, and hence the shorter the distance between the condensation discontinuity and the forerunner dry shock.

Despite these analytical results for the model, whether this model exhibits the ring formation phenomenon (*a*) still remains to be investigated. Furthermore, there is another issue that was overlooked in the early attempts to explain the wave patterns in shock tube experiments: the experimental apparatus in Dettleff *et al.* (1979) and Gulen *et al.* (1994) was rotationally symmetric cylinders. The initial state of the fluid was also cylindrically symmetric. Fluid flow keeps cylindrical symmetry about the centre axis of the cylinder. C.-W. Shu (1999, personal communication) pointed out that the rotational symmetry was broken by those randomly appearing rings. This symmetry breaking is also to be explained.

In this paper, we shall provide an explanation for both the symmetry breaking and ring formation. After the incident shock is reflected, the pressure behind the reflected shock is higher than the equilibrium pressure. Randomly generated liquid or liquid/vapour mixture drops due to nucleation effect then appear and grow behind the reflected shock, breaking the symmetry. These liquid or liquid/vapour mixture drops will evolve into rings of liquid/vapour mixture, with the help of the endwall. This explanation for ring formation is found through the analysis of the motion of the front of a liquid/vapour mixture droplet at the reflection wall and behind the reflected shock. The motion of the liquid droplet's front is governed by the model presented in § 2. The evolution of this droplet into a ring can be explained by features of various types of one-dimensional waves of the model listed in § 3. The explanation is based on the facts that (i) liquid or liquid/vapour mixture droplets are initiated behind the reflected shock, (ii) there is a reflecting wall present, and (iii) the pressure behind the incident dry shock is lower than the equilibrium pressure. These factors coincide with the experimental observation (*a*) nicely. This explanation does not require any bold assumptions (see § 4 for the details of the evolution of a droplet into a ring). The outer front of a ring is a collapsing wave listed in § 3. This suggests that the photographs taken at the end window during experiments provide a way to measure the speeds of collapsing waves. Collapsing waves are supersonic relative to the front of the waves. This is confirmed in § 4 by analysing some rings in photographs published in Gulen *et al.* (1994). The Mach numbers of the rings analysed in § 4 range from 2 to 4.

Our explanation for ring formation also reveals a mechanism for the generation of the 'button' at the centre of a liquefaction shock wave leaving the end of an open-end shock tube, shown in figure 5(*a*), and small-scale asperities on a liquefaction shock wave.

Since the explanation of ring formation relies heavily on the properties of the collapsing waves, we further investigated numerically the sensitivity of their speed to the ratio of species diffusion and typical reaction time, and to the deviation from the equilibrium pressure, as well as to the shapes of the pressure functions. It turns out that the speed of a collapsing wave increases as the ratio of diffusion over reaction time increases, and as the deviation from the equilibrium pressure increases. However, the speed is insensitive to the shapes of pressure functions.

This paper is organized as follows. In § 2, the model developed in Fan (1998, 2000*b*) is presented and discussed. In section § 3, all major one-dimensional waves of the model discovered so far are listed. Two new types of one-dimensional waves for the model, the collapsing and explosion waves, are investigated. These two types of waves cannot exist in the mixed-type p-systems (1.3). It turns out that the outer front of a liquid/vapour mixture droplet behind the reflected shock is a collapsing wave. The explosion waves were studied in Rabie *et al.* (1979) through their model (1.1). In § 4, the symmetry breaking and ring formation are explained in detail. The speeds of collapsing waves are estimated from photographs of experiments to confirm that they are indeed supersonic as predicted by the model. Furthermore, the emergence of the 'button' at the centre of the liquefaction shock front and the small-scale asperities at the liquefaction shock front observed at the exit of the open-end shock tube are also explained in § 4.

2. A model for liquid/vapour phase transitions in shock tube experiments

Let $p_1(\rho, T)$ and $p_2(\rho, T)$ be the pressure function of the pure vapour phase and liquid phase respectively, where ρ is the density and T the temperature. Typical graphs of p_1 and p_2 for fixed temperature are given in figure 6 by thick curves.

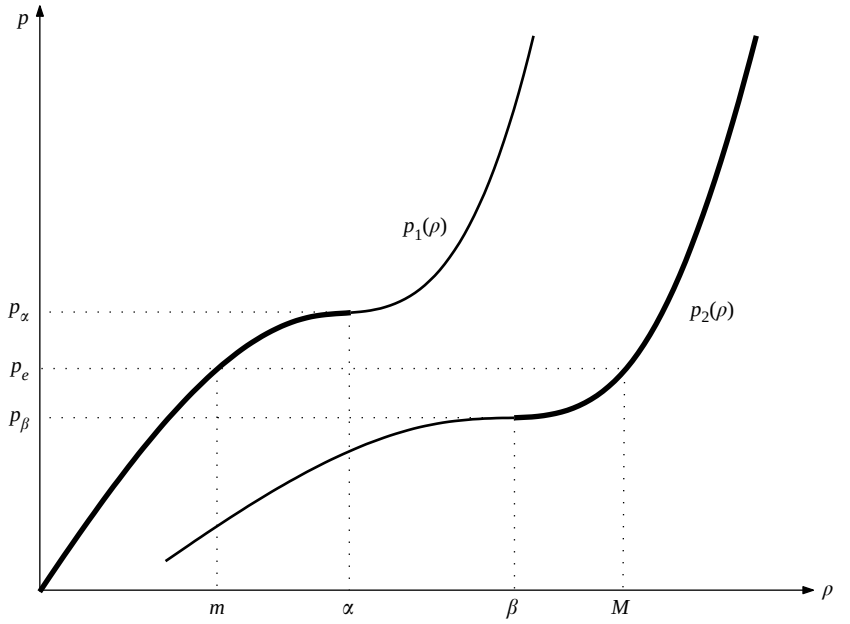

FIGURE 6. Pressure functions $p_1(\rho, T)$ and $p_2(\rho, T)$ for fixed T.

Liquid and vapour phases can coexist in equilibrium at the equilibrium pressure $p = p_e = p_1(m, T) = p_2(M, T)$ where the line joining $(m(T), p_e)$ and $(M(T), p_e)$ is called the Maxwell line. The above quantities and functions can be measured. Each component of function $p(\rho, T)$ is extended continuously to an increasing function on $\mathbb{R}$, as shown in figure 6 by the thin curves, to obtain $p_1(\rho, T)$ and $p_2(\rho, T)$. Although the extended parts of these pressure functions beyond the spinodal limit, i.e. $p_1(\rho_1)$ for $\rho_1 > \alpha$ and $p_2(\rho_2)$ for $\rho_2 < \beta$, cannot be measured and the extension of the pressure function into the spinodal region is somewhat arbitrary, these extended parts of the pressure function do not affect the outcomes. For example, the part of the pressure function $p_1(\rho)$ for $\rho > \alpha(T)$ does not have much effect since there will not be any vapour there.

We shall treat liquid and vapour as different species and specify the transition of phases by a reaction rate equation.

Let quantities a_i, $i = 1, 2$, denote the quantity for vapour when $i = 1$ and that of liquid when $i = 2$. In shock tube experiments, liquid and vapour are finely mixed. The volume fraction of the ith species at point x and time t is $f_i(x, t)$. The density of the ith species in the volume fraction of the ith species at point x and time t is denoted by $\rho_i(x, t)$. The reaction rate function denoting the mass the of ith species produced per unit volume per time unit is w_i. The conservation of mass requires $w_1 + w_2 = 0$.

The model for flows involving liquid/vapour phase transitions used in this paper is derived from the Navier–Stokes systems of equations describing reactive flows:

$$\left.\begin{aligned} &\rho_t + \nabla\cdot(\rho\boldsymbol{u}) = 0,\\ &(\lambda\rho)_t + \nabla\cdot(\lambda\rho\boldsymbol{u}) = w_1 - \nabla\cdot\boldsymbol{j}_1\\ &(\rho\boldsymbol{u})_t + \nabla\cdot(\rho(\boldsymbol{u}\boldsymbol{u}) + \boldsymbol{P}) = 0,\\ &E_t + \nabla\cdot\left(\boldsymbol{u}E + \boldsymbol{u}\cdot\boldsymbol{P} + \boldsymbol{q} + \sum_{i=1}^{2} h_i\boldsymbol{j}_i\right) = 0. \end{aligned}\right\} \tag{2.1}$$

Here $\boldsymbol{u}$ is the average velocity, λ the mass fraction of vapour, ρ the density, E the energy per unit volume, $\boldsymbol{P}$ the stress tensor, $\boldsymbol{q}$ the heat flux vector, $\boldsymbol{j}_i$ the diffusion flux of species i and h_i the specific enthalpy of species i. The function $w_1(\rho, \lambda, T)$ is the rate of vapour creation. The sum of diffusion fluxes of all species satisfies

$$\sum_{i=1}^{2} \boldsymbol{j}_i = \boldsymbol{0}.$$

The energy density is $E = E_1 f_1 + E_2 f_2$ where E_i is the energy density of species i. The energy density E_i can be decomposed further into kinetic energy and internal energy densities:

$$E_i = \tfrac{1}{2}\rho_i u^2 + \rho_i e_i,$$

where $e_i(T, \rho_i)$ is the specific internal energy of species i. The specific enthalpy of species i is

$$h_i = e_i + p/\rho_i.$$

The difference in specific enthalpy of vapour and liquid

$$L(T) = h_1 - h_2$$

represents the heat of formation, or latent heat released when a unit mass of vapour condenses completely to liquid under constant pressure.

The following assumptions simplify the modelling.

(i) Vapour and liquid fill the space, i.e.

$$f_1 + f_2 = 1 \tag{2.2a}$$

$$\rho = \rho_1 f_1 + \rho_2 f_2. \tag{2.2b}$$

(ii) The temperatures of the liquid and vapour components at each point are equal.

(iii) The pressure in the portion occupied by the ith component is $p_i(\rho_i, T)$. Different components at the same location have the same pressure:

$$p = p_1(\rho_1, T) = p_2(\rho_2, T).$$

Thus, the pressure function p can be computed from the following equations:

$$\left.\begin{aligned} p &= p_1(\rho_1, T) = p_2(\rho_2, T), \\ \rho &= \rho_1 f_1 + \rho_2(1 - f_1) \end{aligned}\right\} \tag{2.3}$$

With the notation

$$\lambda := \rho_1 f_1/\rho \tag{2.4}$$

for the mass fraction of the first species and the specific volume v_i of the ith species in the mixture, the system of equations (2.3) becomes

$$\left.\begin{aligned} p &= p_1(v_1) = p_2(v_2), \\ v &= \lambda v_1 + (1 - \lambda) v_2. \end{aligned}\right\} \tag{2.3a}$$

(iv) The stress tensor is

$$\boldsymbol{P} = \left[p + \left(\tfrac{2}{3}\epsilon_1 - \epsilon_2\right)(\nabla \cdot \boldsymbol{u})\right]\boldsymbol{I} - \epsilon_1(\nabla \boldsymbol{u} + \nabla \boldsymbol{u}^T) \tag{2.5}$$

where constants $\epsilon_1, \epsilon_2 > 0$ are viscosity coefficients.

(v) The heat conduction $\boldsymbol{q}$ is given by the Fourier Law

$$\boldsymbol{q} = -\kappa \nabla T \tag{2.6}$$

where $\kappa > 0$ is the heat conductivity coefficient.

(vi) The diffusion flux of the ith species is given by Fick's law:

$$\boldsymbol{j}_i = -\mu\rho\nabla\lambda_i. \tag{2.7}$$

Fick's law is appropriate for a dilute gas. Although fluids in our problem are dense, we still use Fick's law unless there is a better alternative.

Under these assumptions, the system describing the dynamics of phase changes is

$$\left.\begin{aligned} &\rho_t + \nabla\cdot(\rho\boldsymbol{u}) = 0 \\ &(\lambda\rho)_t + \nabla\cdot(\lambda\rho\boldsymbol{u}) = w_1 + \nabla\cdot(\mu\rho\nabla\lambda) \\ &(\rho\boldsymbol{u})_t + \nabla\cdot(\rho(\boldsymbol{uu}) + \boldsymbol{P}) = 0, \\ &E_t + \nabla\cdot(\boldsymbol{u}E + \boldsymbol{u}\cdot\boldsymbol{P}) = \kappa\Delta T + \nabla\cdot(\mu L\rho\nabla\lambda). \end{aligned}\right\} \tag{2.8}$$

Once the relations $e_i = e_i(\rho_i, T)$ and $w_1 = w_1(\rho, \lambda, T)$ are known, the system (2.8) forms a closed system of equations.

In the one-dimensional case, this system is reduced to

$$\left.\begin{aligned} &\rho_t + (\rho u)_x = 0, \\ &(\rho u)_t + (\rho u^2 + p)_x = \epsilon u_{xx}, \\ &E_t + (\rho u E + up - \epsilon u u_x)_x = \kappa T_{xx} + (\mu L(T)\rho\lambda_x)_x, \\ &(\lambda\rho)_t + (\lambda\rho u)_x = w_1 + (\mu\rho\lambda_x)_x. \end{aligned}\right\} \tag{2.9}$$

In Lagrangian coordinates, the corresponding system of equations is

$$\left.\begin{aligned} &v_t - u_x = 0, \\ &u_t + p_x = \epsilon\left(\frac{u_x}{v}\right)_x, \\ &e_t + (up)_x = \epsilon\left(\frac{uu_x}{v}\right)_x + \kappa\left(\frac{T_x}{v}\right)_x + \left(\frac{\mu L(T)\lambda_x}{v^2}\right)_x, \\ &\lambda_t = w(\lambda, v, T) + \left(\frac{\mu\lambda_x}{v^2}\right)_x, \end{aligned}\right\} \tag{2.10}$$

where $w = w_1/\rho$ and e is the specific energy

$$e = \tfrac{1}{2}u^2 + \lambda e_1 + (1-\lambda)e_2.$$

The isothermal case, i.e. when the temperature is constant, of (2.10) is

$$v_t - u_x = 0, \tag{2.11a}$$

$$u_t + p_x = \epsilon\left(\frac{u_x}{v}\right)_x, \tag{2.11b}$$

$$\lambda_t = w(\lambda, v) + \left(\mu\frac{\lambda_x}{v^2}\right)_x. \tag{2.11c}$$

The isothermal model (2.11) approximates the case where heat capacity is very large or where the fluid container is in a heat bath.

In view of (2.3), if $\partial p_1/\partial v$, $\partial p_2/\partial v < 0$, then

$$\frac{\partial p}{\partial v} = \frac{p_1'(v_1)p_2'(v_2)}{\lambda p_2'(v_2) + (1-\lambda)p_1'(v_1)} < 0 \tag{2.12}$$

and

$$\frac{\partial p}{\partial \lambda} = \frac{p_1'(v_1)p_2'(v_2)(v_2 - v_1)}{\lambda p_2'(v_2) + (1-\lambda)p_1'(v_1)} > 0. \tag{2.13}$$

This implies that the left-hand side of (2.11), which is of the form

$$U_t + \boldsymbol{F}(U)_x,$$

is strictly hyperbolic in the sense that $\nabla \boldsymbol{F}(U)$ has three distinct real eigenvalues. In contrast, with the van der Waals pressure function, the system is of hyperbolic–elliptic mixed type, which is, in general, harder to handle than a strictly hyperbolic system. Further calculation shows that

$$\frac{\partial^2 p}{\partial v^2} > 0 \quad \text{if} \quad \frac{\partial^2 p_j}{\partial v^2} > 0, \ \ j = 1, 2. \tag{2.14}$$

The production of the vapour (or liquid) phase occurs through the initiation or annihilation of nuclei of vapour (or liquid) and the subsequent growth of such nuclei when these nuclei and elements of the other phase meet. Thus, the production rate function of the first species is

$$w = w_{growth} + w_{initiation}, \tag{2.15}$$

where $w_{initiation}$ is the rate of the creation of nuclei of the vapour phase, and w_{growth} that of the growth of such nuclei. Arguments similar to the theory of chemical kinetics lead to

$$w_{growth} = k\lambda^a(1-\lambda)^b$$

where a and b are positive constants. In this paper, we shall take

$$w_{growth} = k\lambda(1-\lambda). \tag{2.16}$$

Here $\lambda(1-\lambda)$ is the probability that particles of liquid and vapour collide to make reactions possible and k is the rate constant. In the thermochemistry theory, the rate constant is a function of temperature given by the Arrhenius law. During liquid/vapour phase transitions, however, the temperature changes are usually minor but the rate of phase change varies significantly according to $|p - p_e|$. Thus, the expression for the rate constant k should be adjusted according to the following facts. When $p_e(T) - p(\lambda, v, T) > 0$, where $p_e(T)$ is the equilibrium pressure at temperature T, liquid tends to evaporate and hence $w_{growth} \geqslant 0$. The larger $p_e - p$ is, the faster the evaporation proceeds. Similarly, when $p_e(T) - p(\lambda, v, T) < 0$, vapour tends to condense into liquid and hence $w_{growth} \leqslant 0$, and the larger $|p_e - p|$ is, the faster the condensation occurs. Consistent with these facts, we shall model the growth of nuclei of vapour by

$$w_{growth} = \frac{p - p_e}{\gamma p_e}\lambda(\lambda - 1) \tag{2.17}$$

where γ is taken as a constant. There are some growth rate formulae available in the review article by Kotake & Glass (1981). However, these growth rates are typically too complicated to yield clear insight into ring formation. For a qualitative investigation, we need a growth rate that captures the basic behaviour of the growth rate term, yet allows mathematical analysis to reveal cause–result relations. For this reason, we shall use (2.17) in this paper.

The function $w_{initiation}$, called the nucleation rate, is a complicated topic in itself. For more information on this function, see the review by Oxtoby (1992), Springer (1978)

and references cited therein. The nucleation rate has a significant effect on the speed of, say, a liquefaction wave and its acceleration as shown in Fan (2000*a*). However, to explain the symmetry breaking and ring formation phenomenon, we need only the following qualitative behaviour of the nucleation rate: the nucleation rate is small near the equilibrium pressure, and it is very large near the spinodal limit or Wilson lines. The sign of the nucleation rate for liquid drops is

$$\text{sign}(w_{initiation}) = \text{sign}(p - p_e). \tag{2.18}$$

Remark: The extension part of the pressure functions does not have much effect in our system. For example, consider the part of $p_1(\rho_1)$ in $\rho_1 > \alpha$. In this range, the rate function $w << -1$ has very large absolute value which forces the fraction of vapour λ to be virtually zero in view of (2.11*c*). This implies that $\rho_2 = \rho > \beta$ and hence the pressure $p = p_2(\rho)$ is well-defined and is not sensitive to the extended part of the function p_1 for $\rho_1 > \alpha$.

Remark: The term $(\lambda_x/v)_x$ represents the diffusion of vapour species into the mixture of vapour and liquid. The diffusion effect not only exists naturally, but also has a significant role in the system (2.11) and hence (2.8). The term $(p - p_e)\lambda(\lambda - 1)/\gamma/p_e$ represents the rate of reaction for liquid and vapour particles at the same location (x, t) only. It does not cover the reaction among neighbouring particles. The diffusion term $\mu\lambda_{xx}$ then determines the probability that neighbouring particles collide. The necessity of this diffusion term can be illustrated by the following example. Let $u = 0$, $T =$ constant,

$$\lambda = \begin{cases} 0, & x < 0, \\ 1, & x \geqslant 0, \end{cases}$$

and v be such that the pressure is a constant larger than p_e at the initial time. By the Maxwell rule, which states that the only stationary phase boundary happens at the equilibrium pressure, vapour should start to condense at the liquid/vapour interface which results in the motion of the phase boundary. However for the system (2.11) with $\mu = 0$ the solution is the initial data and hence no phase change happens. On the other hand, when the pressure is not the equilibrium pressure, the liquid/vapour interface in (2.11) with $\mu > 0$ must move, which is in agreement with the Maxwell rule.

There are many droplet growth formulae available, see Kotake & Glass (1981) and references therein for information. These formulae already include the effect of vapour near a droplet of liquid colliding with the droplet, resulting in the growth of the droplet. Thus, in the systems of phase transition flows mentioned in Kotake & Glass (1981), there are no diffusion terms for species. On the other hand, the growth rate (2.17) does not include the effect of diffusion and hence a diffusion term is needed.

3. Basic one-dimensional isothermal waves

The isothermal system (2.11) describes fluid evolution in an apparatus immersed in a heat bath. It is an approximation for retrograde fluids since the temperature does not change much in shock tube experiments due to their high heat capacity. Any results in the isothermal case can serve as guides for the non-isothermal system. For the isothermal system, the analysis is easier and waves can be shown clearly on (p, v)-diagrams. When significant differences between the behaviour of waves of the

isothermal system (2.11) and that of the non-isothermal one (2.10) are expected, we shall point them out.

The isothermal system (2.11) contains three positive parameters: viscosity ϵ, typical reaction time γ, and diffusion coefficient μ. These three parameters are proportional to the mean free path. Thus, for simplicity, we shall assume these three parameters are constant, and use the scaling $\gamma = \epsilon/A$ and $\mu = B\epsilon$. For convenience of mathematical analysis, we change the diffusion terms $(u_x/v)_x$ and $(\lambda_x/v)_x$ to u_{xx} and λ_{xx} respectively. Then, the system (2.11) becomes

$$\left.\begin{aligned} &v_t - u_x = 0, \\ &u_t + p(v, \lambda)_x = \epsilon u_{xx}, \\ &\lambda_t = \frac{A}{\epsilon}(p - p_e)\lambda(\lambda - 1) + B\epsilon\lambda_{xx}, \\ &(u, v, \lambda)(x, 0) = \begin{cases} (u_-, v_-, \lambda_-) & \text{if } x < 0, \\ (u_+, v_+, \lambda_+) & \text{if } x > 0. \end{cases} \end{aligned}\right\} \tag{3.1}$$

Note that the nucleation term is omitted in (3.1) to concentrate on the propagation of phase boundaries without the influence of nucleation terms. Later we can consider the effects of adding in the nucleation term. One of the results in Fan (2000*a*) states that the inclusion of the nucleation term will accelerate the propagation of the phase boundaries. The effect of a modification of the viscosity and diffusion terms will be discussed later.

Typical reaction times $\epsilon/A > 0$ are very small. This motivates us to consider the zero reaction time limit $\epsilon \to 0$ of solutions of (3.1). Denote the solution of (3.1) by $(u^\epsilon, v^\epsilon, \lambda^\epsilon)(x, t)$. If there is a sequence ϵ_n, $n = 1, 2, \ldots$, such that $\epsilon_n \to 0+$ as $n \to \infty$ and the limit

$$(u, v, \lambda)(x, t) := \lim_{n\to\infty}(u, v, \lambda)(x, t) \tag{3.2}$$

exists almost everywhere, then in the sense of distributions the limit satisfies

$$v_t - u_x = 0, \tag{3.3a}$$

$$u_t + p(v, \lambda(x, t))_x = 0, \tag{3.3b}$$

$$(p(v, \lambda) - p_e)\lambda(\lambda - 1) = 0, \tag{3.3c}$$

$$(u, v, \lambda)(x, 0) = \begin{cases} (u_-, v_-, \lambda_-) & \text{if } x < 0, \\ (u_+, v_+, \lambda_+) & \text{if } x > 0. \end{cases} \tag{3.3d}$$

The structures of solutions of (3.3) are easier to characterize than those of (3.1). Due to (3.3*c*), any smooth part of a solution of (3.3) must either have constant $\lambda = 0, 1$ or constant pressure $p = p_e$. The latter is called an isobaric wave. For a non-isobaric wave to have $\lambda(x, t)$ varying with x, discontinuities in $\lambda(x, t)$ must be introduced.

There are two basic types of waves for (3.3): reacting and non-reacting. Reacting waves are those solutions of (3.1) involving phase changes after the waves pass through the fluid. From the last paragraph, basic reacting waves are either isobaric waves or step functions, called shocks,

$$(u, v, \lambda)(x, t) = \begin{cases} (u_+, v_+, \lambda_+) & \text{if } x - ct > 0, \\ (u_-, v_-, \lambda_-) & \text{if } x - ct < 0, \end{cases} \tag{3.4}$$

where the constant c is the shock speed determined by the Rankine–Hugoniot condition

$$\left.\begin{aligned} -c(v_+ - v_-) - (u_+ - u_-) &= 0, \\ -c(u_+ - u_-) + (p_+ - p_-) &= 0. \end{aligned}\right\} \tag{3.5}$$

Since the structures of solutions of (3.3) are easier to characterize, we can study the behaviour of (3.1) through the behaviour of solutions of (3.3) which are the $\epsilon \to 0+$ limits of solutions of (3.1). However, some solutions of (3.3) are not the $\epsilon \to 0+$ limits of solutions of (3.1) and hence they do not approximate solutions of (3.1) when $\epsilon > 0$ is small. This motivates the following vanishing-viscosity admissibility criterion for solutions of (3.3):

DEFINITION 3.1. *A solution* $(u, v, \lambda)(x, t)$ *of* (3.3) *is admissible if there is a sequence* $\{\epsilon_n\}_{n=1}^{\infty}$, *with* $\epsilon_n \to 0+$ *as* $n \to \infty$ *such that*

$$(u, v, \lambda)(x, t) = \lim_{n\to\infty} (u^{\epsilon_n}, v^{\epsilon_n}, \lambda^{\epsilon_n})(x, t) \tag{3.6}$$

where $(u^{\epsilon_n}, v^{\epsilon_n}, \lambda^{\epsilon_n})$ *are solutions of* (3.1) *with* $\epsilon = \epsilon_n$.

Remark: In the above definition, we choose pointwise convergence for the purpose of definiteness. Other types of strong limits can also be used.

A travelling wave of (3.1) is a solution of (3.1) of the form

$$(u, v, \lambda)\left(\frac{x - ct}{\epsilon}\right)$$

where c is the wave speed relative to the Lagrangian coordinate, i.e. wave speed relative to fluid particles. It satisfies

$$\left.\begin{aligned} &-cv' - u' = 0, \\ &-cu' + p' = u'', \\ &-c\lambda' = Aw(v, \lambda) + B\lambda'', \\ &(v, u, \lambda)(\pm\infty) = (v_\pm, u_\pm, \lambda_\pm), \quad (v', u', \lambda')(\pm\infty) = (0, 0, 0). \end{aligned}\right\} \tag{3.7}$$

After some simplification, system (3.7) becomes

$$\left.\begin{aligned} &-cv' = c^2(v - v_-) + p - p_-, \\ &-c\lambda' = Aw(v, \lambda) + B\lambda'', \\ &(v, \lambda)(-\infty) = (v_-, \lambda_-), \quad (v, \lambda)(\infty) = (v_+, \lambda_+). \end{aligned}\right\} \tag{3.8}$$

An asymptotic analysis shows that for a shock solution (3.4) to satisfy the vanishing-viscosity admissibility criterion, it is necessary that (3.8) has a solution. Conversely, if the shock data (3.4) are such that (3.8) has a solution, then this shock satisfies the vanishing-viscosity criterion. This leads to the following travelling wave admissibility criterion:

DEFINITION 3.2. (*a*) *We say that a shock* (3.4) *is admissible by the travelling wave criterion* (*or say that the shock has a travelling wave profile*), *if* (3.8) *has a solution.* (*b*) *A piecewise continuous solution of* (3.2) *is said to be admissible by the travelling wave criterion if all discontinuities in the solution are admissible in the sense of* (*a*).

Working with the vanishing-viscosity admissibility criterion, Definition 3.1, directly is usually very difficult and expensive. Thus, we shall use the travelling wave criterion.

According to (3.3*c*) and the Rankine–Hugoniot conditions (3.5), there are the following cases with non-negative wave speeds c. The case for negative wave speeds can be obtained by a change of coordinate, $x \mapsto -x$.

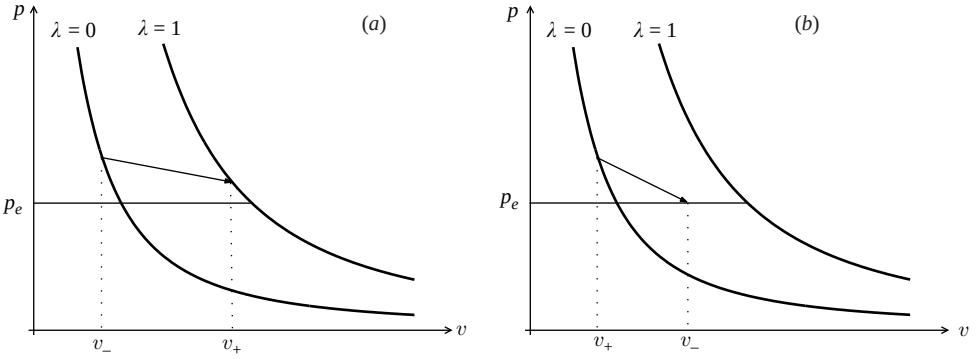

FIGURE 7. Pressure function $p(v, \lambda)$: case 1.

Case 1. Liquefaction wave. The system (2.11) has travelling waves with either (*a*) $\lambda_- = 0$, $\lambda_+ = 1$, $v_- < v_+$ and $p(v_-, \lambda_-) > p(v_+, \lambda_+) \geqslant p_e$, or (*b*) $\lambda_- = 0$, $0 < \lambda_+ < 1$, $v_- < v_+$ and $p(v_-, \lambda_-) > p(v_+, \lambda_+) = p_e$ (see figure 7).

In front of the wave, the fluid is vapour in case (1*a*) and liquid/vapour mixture in case (1*b*). Behind the shock, the fluid is liquid, because $\lambda_- = 0$. After the wave passes, the fluid becomes liquid. Thus, this wave is called a liquefaction wave. Fan (1998, 2000*b*) proved that liquefaction waves exist if the wave speeds satisfy

$$c = \sqrt{-\frac{p(v_+, \lambda_+) - p(v_-, \lambda_-)}{v_+ - v_-}} \geqslant 2\sqrt{AB|p(v_-, \lambda_-) - p_e|}. \tag{3.9}$$

On the other hand, if the speeds satisfy

$$c \leqslant 2\sqrt{AB|p(v_+, \lambda_+) - p_e|}, \tag{3.10}$$

then there is no travelling wave. Note that in case 1(*b*), the condition (3.10) does not impose any restriction. Numerical computations show that for case 1(*b*), there is always a travelling wave as long as $\lambda_+ \in (0, 1)$, even if (3.9) is not satisfied.

In the non-isothermal case, liquefaction waves are typically partial, meaning that $\lambda_- > 0$, i.e. the fluid behind the wave is a mixture of liquid and vapour. This is because as vapour condenses to liquid, latent heat is released, which raises the temperature T_- behind the wave. The equilibrium pressure $p_e(T_-)$ will increase as the temperature rises to reach the pressure behind the wave, p_-. When $p_e(T)$ reaches p_-, the condensation will stop, resulting in partial liquefaction, i.e. $1 > \lambda_- > 0$ and $p(v_-, \lambda_-, T_-) = p_e(T_-)$. By contrast, this mechanism is absent in the isothermal case, and hence only complete liquefaction waves are present.

Case 2. Evaporation waves. Fan (1998, 2000*b*) also proved that under the same existence condition (3.9), there are travelling waves of (2.11) with either (*a*) $\lambda_- = 1$, $\lambda_+ = 0$, $v_- > v_+$ and $p(v_-, \lambda_-) < p(v_+, \lambda_+) \leqslant p_e$, or (*b*) $\lambda_- = 1$, $1 > \lambda_+ > 0$, $v_- > v_+$ and $p(v_-, \lambda_-) < p(v_+, \lambda_+) = p_e$ (see figure 8). After the wave passes the fluid, the fluid changes from liquid, or liquid/vapour mixture, to vapour. Thus, this wave is called an evaporation wave. Similarly, under condition (3.10), there is no evaporation wave. Our numerical tests show that there is a travelling wave for case 2(*b*) as long as $\lambda_+ \in (0, 1)$, even if (3.9) is not satisfied.

In the non-isothermal case, evaporation waves are usually partial, meaning that $1 > \lambda_- > 0$ and $p(v_-, \lambda_-, T_-) = p_e(T_-)$.

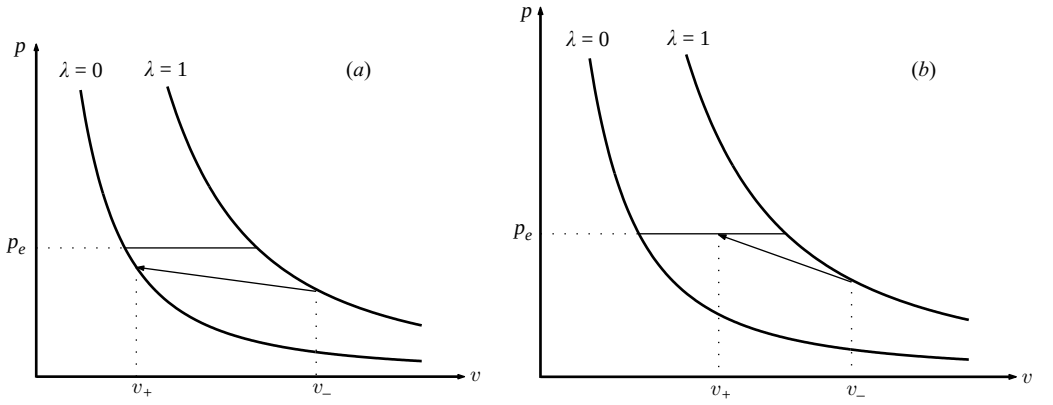

FIGURE 8. Pressure function $p(v, \lambda)$: case 2.

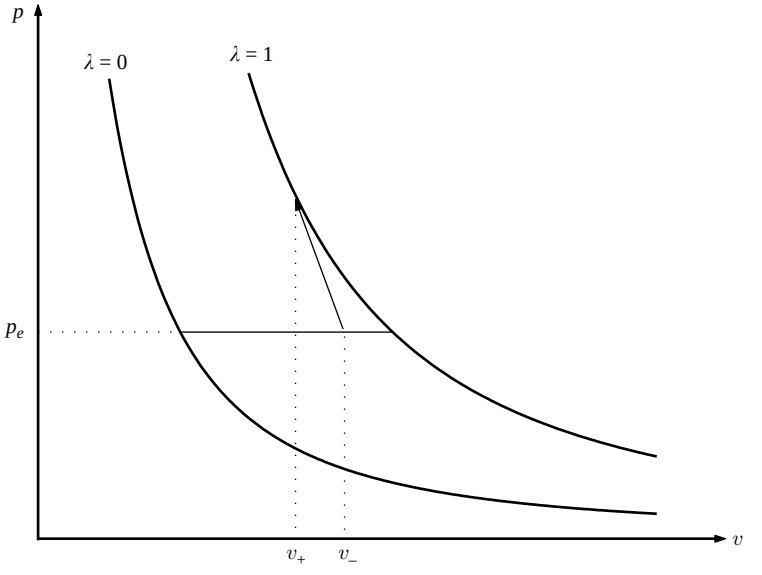

FIGURE 9. Pressure function $p(v, \lambda)$: case 3.

Case 3. Collapsing wave. In front of this wave is a metastable vapour, $\lambda_+ = 1$, $p_+ > p_e$. Behind the wave is a liquid/vapour mixture at equilibrium pressure, $p_- = p_e$, $\lambda_- \in (0, 1)$, as shown in figure 9. As fluid passes through the wave, it undergoes fast condensation. The existence of this kind of wave is verified by numerical computations. The pressure function in (3.1) used in the numerical study is

$$p(v, \lambda) = \frac{(1 + \lambda)^2}{4v^2}. \tag{3.11}$$

The equilibrium pressure is $p_e = 1$ and the Maxwell lines are $m = 1/2$ and $M = 1$. For the right-hand side of (3.1), centred differences are utilized for the second-order derivative terms and an explicit scheme for the reaction term. To reduce the influence of numerical viscosity from the discretization of the left-hand side of (3.1), the

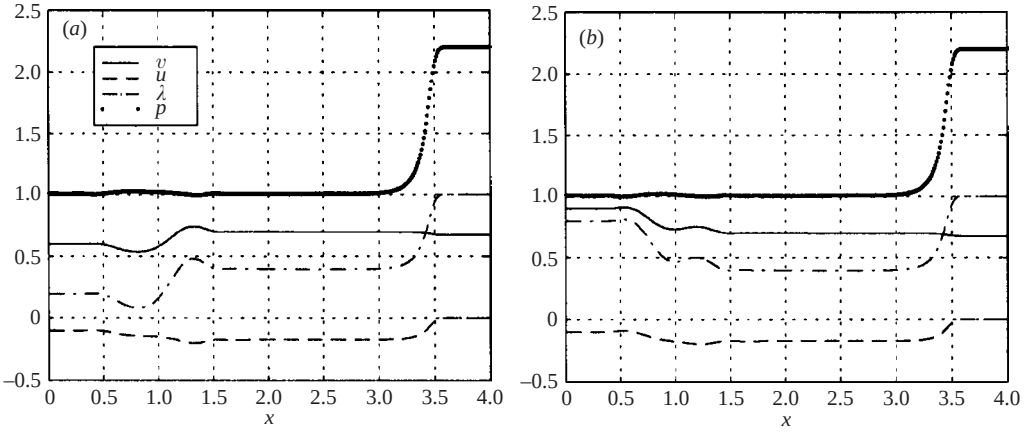

FIGURE 10. (*a*) The solution of (3.1) with $\mu = 10\gamma$, and initial data (3.12) where $p_+ = p_e + 1.2$, $\lambda_+ = 1$, $p_- = p_e$, $v_- = 0.6$, $\lambda_- = 0.2$. The speed of the collapsing wave near the location $x = 3.5$ is calculated through the Rankine–Hugoniot conditions with data at $x = 2.5$ and $x = 4$. (*b*) As (*a*) except that $v_- = 0.9$, $\lambda_- = 0.8$. The speeds of the collapsing wave in (*a*) and (*b*) are the same.

$p_+ - p_e$	s_s	s_2	s_{10}
1.2	2.555	3.689	6.965
1.0	2.378	3.309	6.328
0.8	2.20	2.897	5.628
0.6	2.020	2.440	4.841
0.4	1.820	1.892	3.914
0.2	1.621	NCW	2.712

TABLE 1. Speed of collapsing waves for various $p_+ - p_e$ when the pressure function is (3.11). Here, s_s is the sound speed at $(v_+, \lambda_+ = 1)$, s_2 the speed of the collapsing wave when $\mu = 2\gamma$, s_{10} the speed of the collapsing wave when $\mu = 10\gamma$ and NCW means no collapsing wave. Grid size parameters for computations are $\Delta x = 0.01$ and $\Delta t = 1.41421 \times 10^{-5}$.

third-order WENO discretization proposed by Jiang & Shu (1996) is used for the left-hand side of (3.1). Initial data for computations are

$$(v, u, \lambda)(x, t) = \begin{cases} (v_+, 0, 1) & \text{if } x > 1, \\ (v_-, -0.1, \lambda_-) & \text{if } x < 1, \end{cases} \tag{3.12}$$

where

$$p_- = p(v_-, \lambda_-) = p_e = 1, \quad 0 < \lambda_- < 1 \quad \text{and} \quad p(v_+, 1) > p_e$$

By choosing $u_+ = 0$, the value of (v_+, λ_+) and the front states of the collapsing wave coincide. After sufficiently many time steps, the collapsing wave profile appears as shown in figure 10. The speed of the collapsing wave does not depend on (v_-, λ_-) as long as $p_+ - p_e$ is fixed and $p(v_-, \lambda_-) = p_e$ and $0 < \lambda_- < 1$. The computed results are tested for stability with respect to grid sizes by varying Δt and Δx with $\Delta t/\Delta x^2 \leqslant 0.5$. The results are recorded in table 1.

Table 1 shows that speeds of collapsing waves are faster when the species diffusion coefficient μ increases and when the difference $p_+ - p_e$ increases. This coincides with

$p_+ - p_e$	s_s	s_2	s_{10}
1.2	2.2	3.699	NCW
1.0	2.0	3.32	6.34
0.8	1.8	2.91	5.638
0.6	1.6	2.456	4.849
0.4	1.4	1.934	3.921
0.2	1.2	1.285	2.722
0.1	1.1	NCW	1.888

TABLE 2. Speed of collapsing waves for various $p_+ - p_e$ when the pressure function is (3.13). Grid size parameters for computations are $\Delta x = 0.01$ and $\Delta t = 2 \times 10^{-5}$.

the intuition that when the species diffusion coefficient μ is larger, more vapour/liquid mixture in the back of the wave diffuses to the front of the wave, which is in the metastable vapour state. This causes the metastable vapour in front of the wave to condense faster, which makes the wave move faster. Table 1 also shows that collapsing waves are supersonic relative to their fronts. The Mach number of the collapsing wave increases as $p_+ - p_e$ increases.

To test the dependence of the speeds of collapsing waves on the shape of the pressure functions, we used the pressure function

$$p(v, \lambda) = \frac{1 + \lambda}{2v} \tag{3.13}$$

in table 2. Tables 1 and 2 show that speeds of collapsing waves are almost insensitive to the shapes of pressure functions as long as such waves exist for both pressure functions.

Case 4. Explosion wave. In front of the wave is a metastable liquid, $\lambda_+ = 0$, $p_+ < p_e$. Behind the wave is a liquid/vapour mixture at equilibrium pressure, $p_- = p_e$, $\lambda_- \in (0, 1)$. The Rankine–Hugoniot conditions then require $v_+ > v_-$ as depicted in figure 11. As the wave passes through the fluid, evaporation occurs and the pressure increases. The wave speed is faster than the frozen sound speed. Like the collapsing wave in case 3, we have not analytically proved the existence of this kind of wave, but verified it numerically.

Case 5. Isobaric wave. The term isobaric wave refers to the region of a solution of (3.3) where $p \equiv p_e$. For example, when the isothermal liquid/vapour mixture at equilibrium is compressed, condensation will occur but the pressure stays at equilibrium. A more explicit form of isobaric wave arises from $p \equiv p_e$ and (3.3):

$$\left.\begin{aligned} &u = u(x, t_0), \\ &v(x, t) = v_t(x, t_0)(t - t_0) + v(x, t_0), \\ &\lambda = \lambda_e(v(x, t)). \end{aligned}\right\} \tag{3.14}$$

Whether some solutions of the form (3.14) are not admissible and how to select admissible solutions from (3.14) are left for future research.

Non-reacting waves are solutions of (3.3) where there is no net change of phase before and after waves pass through the fluid.

Case 6. Non-reacting compressive shock waves. In the case where $p_{vv} > 0$, a non-reacting shock must satisfy $\lambda_- = \lambda_+ = 0$ or 1 and the Lax admissibility conditions

$$\sqrt{-p_v(v_-, \lambda_-)} > c > \sqrt{-p_v(v_+, \lambda_+)}, \tag{3.15a}$$

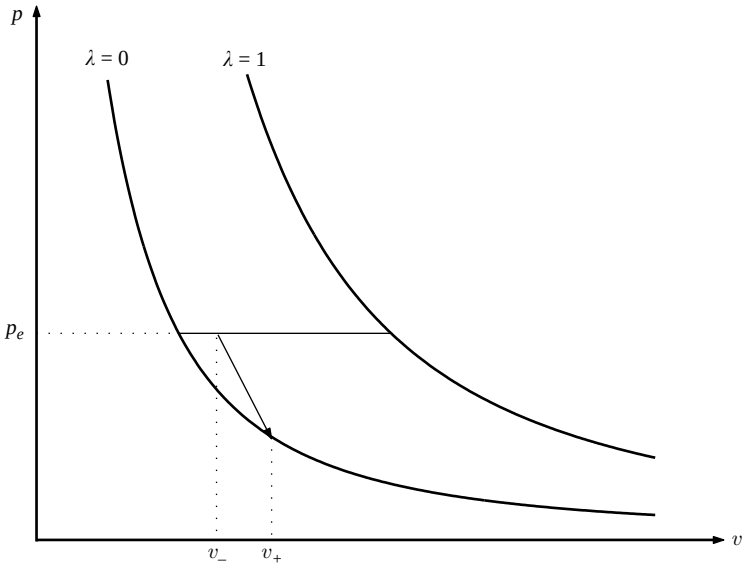

FIGURE 11. Pressure function $p(v, \lambda)$: case 4.

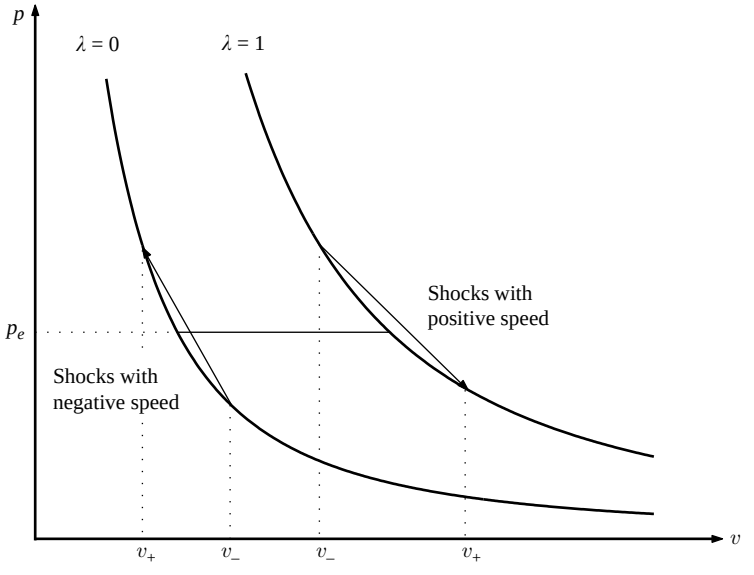

FIGURE 12. Pressure function $p(v, \lambda)$: case 6.

or

$$-\sqrt{-p_v(v_-, \lambda_-)} > c > -\sqrt{-p_v(v_+, \lambda_+)}, \tag{3.15b}$$

where c is the wave speed determined by the Rankine–Hugoniot conditions (see figure 12).

Case 7. Non-reacting rarefaction waves. These are continuous solutions of (3.3), (3.4) of the form $(u, v, \lambda)(x, t) = (u, v, \lambda)(x/t)$. By (3.3$c$), it is necessary that $\lambda(x, t) \equiv$

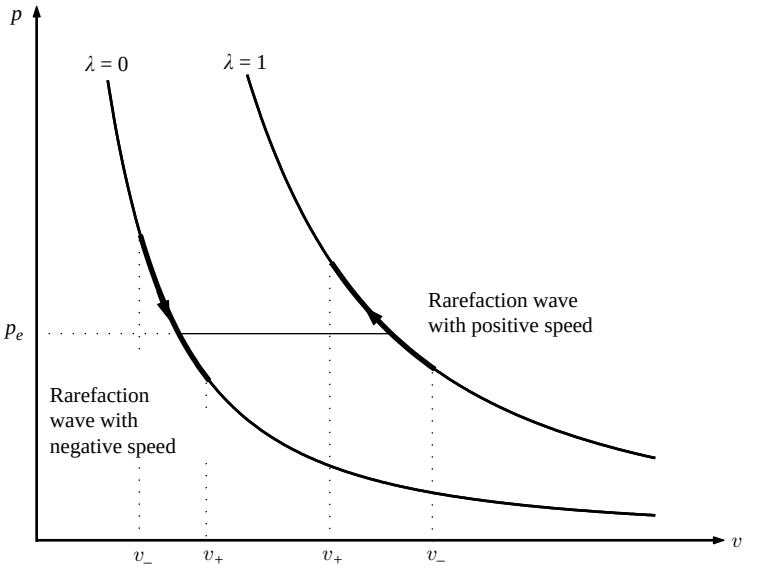

FIGURE 13. Pressure function $p(v, \lambda)$: case 7.

$\lambda_\pm = 0$ or 1, and the system (3.3) is reduced to the non-reacting p-system for gas dynamics. In order for (3.3) with (3.4) to have a rarefaction wave solution, it is necessary and sufficient that

$$u_+ - u_- = \int_{v_-}^{v_+} \sqrt{-p_v(v, \lambda_-)}\, dv, \quad v_- < v_+ \quad \text{(first family of rarefaction waves)} \tag{3.16}$$

or

$$u_+ - u_- = -\int_{v_-}^{v_+} \sqrt{-p_v(v, \lambda_-)}\, dv, \quad v_- > v_+ \quad \text{(second family of rarefaction waves),} \tag{3.17}$$

as shown in figure 13.

Recall that the above results are for the system (3.1) with the viscosity and diffusion terms modified from (2.11). For non-reacting waves as described in cases 6 and 7, such a modification has no effect on the wave speed and the end states since they are determined algebraically by the Lax criterion and the Rankine–Hugoniot conditions. For the reactive waves, described in cases 1 to 5, we expect that such a modification will change the wave speed, because the modification changes the ratio of the effective diffusion coefficient over typical reaction time γ. The larger this ratio is, the faster the phase boundary moves. However, the qualitative behaviours for end states of phase boundaries as shown in figures 6, 7, 8, and 11 are expected to remain the same under this modification, as confirmed by our numerical experiments.

4. Symmetry breaking and ring formation

In this section, we shall give an explanation of the symmetry breaking and ring formation during the shock tube experiments on retrograde fluids. In shock tube experiments, a glass window closes one end of the tube, as depicted in figure 2. The

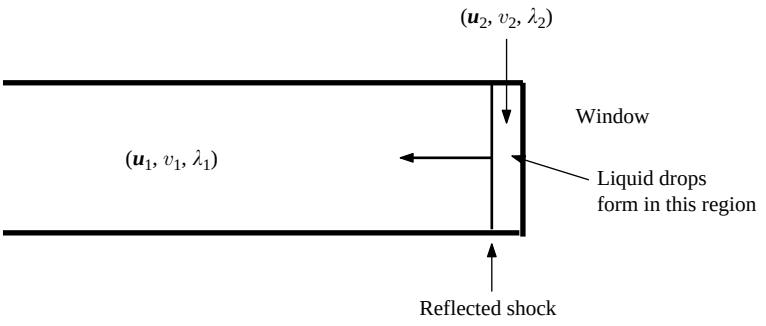

FIGURE 14. The moment after the shock is reflected by the endwall. The state $(\boldsymbol{u}_1, p_1, \lambda_1)$ in front of the reflected shock is chosen to be $\lambda_1 = 1$, $p_1 < p_e$, and the velocity of the fluid $\boldsymbol{u}_1 = u_1\boldsymbol{k}$ with $u_1 < 0$. The state behind the shock satisfies $\boldsymbol{u}_2 = u_2\boldsymbol{k}$, $p_2 > p_e$, $\lambda_2 = 1$).

tube is filled with a stable vapour of retrograde fluid. The piston on the left is pushed into the tube to send a compressive shock wave into the vapour. After the shock is reflected by the endwall, a reflected shock travelling away from the wall will form. The initial pressure of the vapour and the speed of the piston are chosen so that the pressure of the fluid after the incoming shock, p_1, is still below the equilibrium pressure, and the pressure after the reflected shock, p_2, is above equilibrium pressure (see figure 14). Rings of liquid/vapour mixture will appear at the window first and then quickly spread out behind the reflected shock. The experiment apparatus is cylindrically symmetric around the centre axis of the shock tube. The appearance of many liquid/vapour mixture rings clearly breaks the symmetry. This raises the question of the cause of the symmetry breaking.

The symmetry breaking can be explained as follows. Just after the shock is reflected, the pressure behind the reflected shock p_2 is higher than the equilibrium pressure. By fluctuations, liquid droplets appear randomly behind the reflected shock. Since the pressure $p_2 > p_e$, these liquid droplets will grow. The growth is fast when the pressure p_2 is close to the Wilson line. Then the temperature inside and near these droplets will increase due to the latent heat released as the vapour condenses on the droplets. The increased temperature will raise the equilibrium pressure $p_e(T)$, while the pressure in the droplets will decrease due to the condensation. Then the liquefaction process will stop halfway when the equilibrium pressure and pressure in the droplets become equal, resulting in partial liquefaction, or liquid/vapour mixture. This consideration yields the reason for symmetry breaking behind the reflected shock: the combination of the randomness of locations of liquid droplets initiated and the subsequent growth of these droplets, especially when p_2 is close to the Wilson line.

The above argument only explains the symmetry breaking. To see why rings of liquid/vapour mixture are formed, more detailed analysis is required. To this end, we concentrate on the evolution of one liquid/vapour mixture droplet behind the reflected shock wave. Figure 15 depicts, with cylindrical symmetric coordinates (r, z), the states of fluid near such a drop just after it is created. Inside the liquid/vapour mixture drop, the state is $(p, \lambda) = (p_e, \lambda_3)$ with $1 > \lambda_3 > 0$. When the droplet forms, the pressure inside the droplet decreases from p_2 to $p_3 = p_e$ and hence the velocity of fluid in the droplet in the radial direction $\boldsymbol{r}$ will change from 0 to negative, i.e. $\boldsymbol{u}_3 \cdot \boldsymbol{r} < 0$. Outside the droplet, the state of the fluid is $(p_2, \lambda_2) = (p_2 > p_e, 1)$. The Riemann solver for this type of initial data consists of a collapsing shock, as is shown in case 3 of § 3 and figure 10, and some other less visible waves. The front of the drop

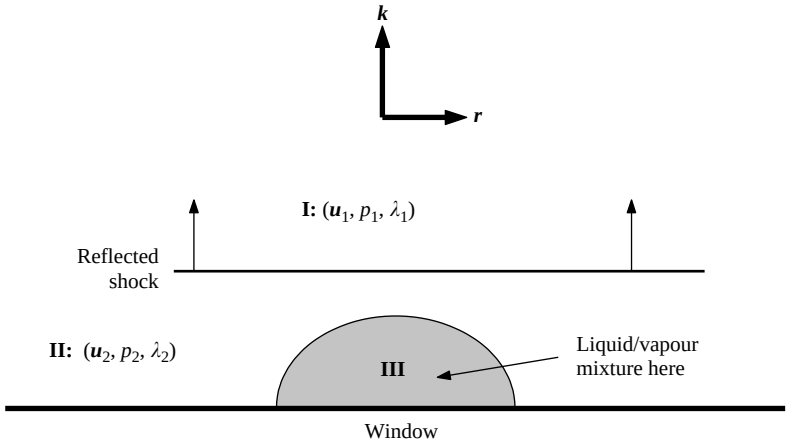

FIGURE 15. The initial state around a drop of liquid/vapour mixture: $\boldsymbol{r}, \boldsymbol{k}$ are the directions of axes of the cylindrical symmetric coordinate. Region III is a drop of liquid/vapour mixture with state $(\boldsymbol{u}_3, p_3, \lambda_3)$ Here, $0 < \lambda_3 < 1$, $p_1 < p_3 = p_e < p_2$, $\boldsymbol{u}_3 \cdot \boldsymbol{r} < \boldsymbol{u}_1 \cdot \boldsymbol{r} = \boldsymbol{u}_2 \cdot \boldsymbol{r} = 0$.

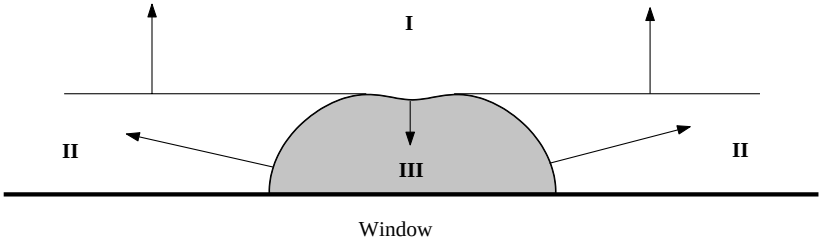

FIGURE 16. The state of the fluid after the front of the drop contacts region I. The front $\mathrm{I} \rightarrow \mathrm{III}$ moves into the region III.

will evolve as a collapsing wave. The collapsing wave in one dimension propagates faster than the frozen sound speed $\sqrt{-p_v(v_2, \lambda_2)}$, while the reflected shock $\mathrm{II} \rightarrow \mathrm{I}$ is slower than $\sqrt{-p_v(v_2, \lambda_2)}$. By a remark later in this section, we shall see that the cylindrical symmetry and the non-positive $\boldsymbol{u}_3 \cdot \boldsymbol{r}$ will further increase the speed of the collapsing wave. Thus, the front of the drop will quickly catch up with the shock $\mathrm{II} \rightarrow \mathrm{I}$, as shown in figure 16. Here, the arrow in $\mathrm{II} \rightarrow \mathrm{I}$ indicates that the front of the wave is region I and the back of the wave is region II. After the front of the drop catches the reflected shock, the front of the liquid/vapour mixture drop has two parts. The first part is the boundary between regions I and III, and the second part is that between III and II. The state of fluid behind $\mathrm{I} \rightarrow \mathrm{III}$ is $(v, \lambda, p) = (v_1, 1, p_1)$ while that in front of the second part is $(v, \lambda, p) = (v_2, 1, p_2)$ (see figure 16). Since $p_3 = p_e > p_1$, the shock $\mathrm{I} \rightarrow \mathrm{III}$ separating regions I and III is an evaporation wave described in case 2 of § 3. Since the speed of fluid behind the reflected shock is close to zero, the front $\mathrm{I} \rightarrow \mathrm{III}$ moves toward the reflecting wall. Meanwhile, the front $\mathrm{III} \rightarrow \mathrm{II}$ separating regions II and III continues to move into region II, as shown in figure 16. The speed of the front $\mathrm{III} \rightarrow \mathrm{II}$ is faster than the sound speed at $(v_2, \lambda_2 = 1)$, $\sqrt{-p_v(v_2, 1)}$ since it is a collapsing wave. The speed of the evaporation shock $\mathrm{I} \rightarrow \mathrm{III}$ is slower than the sound speed at $(v_1, \lambda = 1)$, $\sqrt{-p_v(v_1, 1)}$. Under the assumption that $p_{vv} > 0$, the speed

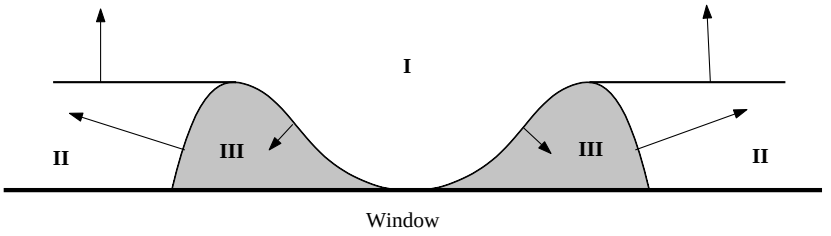

FIGURE 17. A ring forms after the front I → III contacts the window endwall.

$\sqrt{-p_v(v_1, 1)}$ is less than $\sqrt{-p_v(v_2, 1)}$. Thus, the motion of the front I → III cannot kill the liquid/vapour mixture region as long as the front III → II remains a collapsing wave. The front III → II can cease to be a collapsing wave if $p_e(T_3)$ becomes not less than p_2. This is possible if the latent heat is large and the heat capacity is small, as in the case of regular fluids, so that the temperature T_3 becomes high enough to push $p_e(T_3)$ above p_2. Retrograde fluids have high heat capacities and hence region III will remain. On the other hand, for regular fluids, region III may vanish. After a part of the front I → III reaches the window wall, a ring of liquid/vapour mixture appears, as illustrated by figure 17.

Remark. The cylindrical symmetry will not make the speed of the collapsing wave front III → II in figure 16 slower than in the one-dimensional case. First of all, the wave speed is determined by the Rankine–Hugoniot conditions:

$$c = \sqrt{-\frac{p_2 - p_3}{v_2 - v_3}}. \tag{4.1}$$

Thus, the speed c only depends on the value of p and v on the two sides of the front. The cylindrical symmetry affects the values of p and v on the two sides of the front. The initial velocity of the fluid in the radial direction is zero. As the front III → II passes, the radial velocity of the fluid behind the front will move towards the centre z-axis. This will make the fluid inside region III denser while the pressure will remain at the equilibrium value $p_3 = p_e(T)$ due to the fast reaction in liquid/vapour mixture. The compression effect in III will raise the temperature T and hence $p_3 = p_e(T)$. But because the fluid is retrograde, the temperature change is small. The denser v_3 is closer to v_2 than in the one-dimensional case while $p_3 - p_2$ differs a little from the one-dimensional case. Then in view of the Rankine–Hugoniot conditions, the speed of the front c will not become less than that in the one-dimensional case.

The above analysis on the formation of rings implies that the outer fronts of rings are collapsing shock waves. This suggests that it is possible to determine the speed of the collapsing waves from photographs taken at the end window of the shock tubes. It is interesting to see whether the outer fronts of rings of cloud propagate supersonically as predicted by case 3 of § 3. An example of such photographs is figure 18 of Gulen *et al.* (1994), which is copied here as figure 18. The diameter of the window is 57.4 mm.

Example 4.1. In figure 18(*e*), the radius of the largest ring of cloud pointed out by the white arrow is about 6.8 mm. Although the photograph does not show when this ring is initiated, it certainly takes less than 20 μs to form such a ring. Assume this ring grew from a tiny liquid/vapour drop. Then the average speed of the outer front of the ring is not less than 340 m s^{-1}. Gulen *et al.* (1994) stated that the sound speed

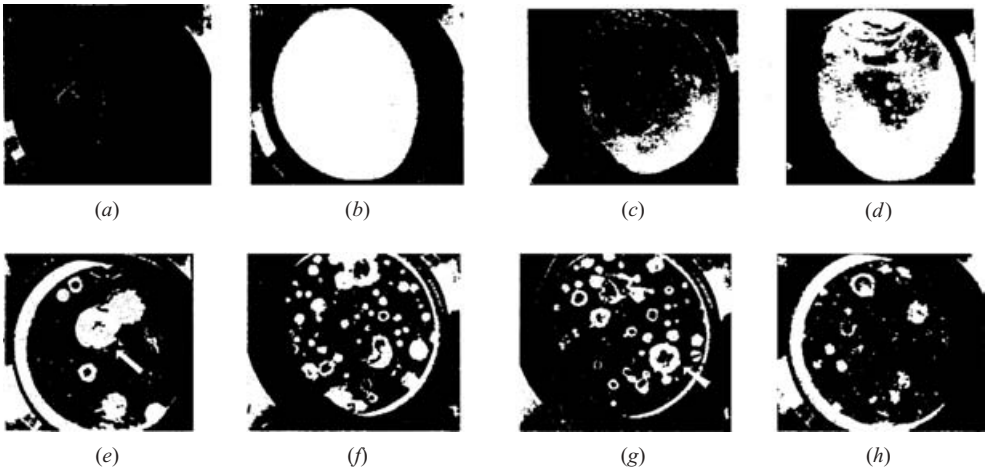

FIGURE 18. Photographs of rings of liquid/vapour mixture behind the reflected (liquefaction) shock wave obtained by Gulen *et al.* (1994). The fluid used is iso-octane. The parameters are $p_0 = 0.402$ bar, $T_0 = 100\,^{\circ}$C. (*e*) Test #oct051490-2: incident shock's Mach number is $M_0 = 2.81$. The photograph was taken at $t_d = 20.0\,\mu$s after the incident shock reached the end window. (*g*) Test #oct051590-3: $M_0 = 2.87$, $t_d = 6.0\,\mu$s.

of the fluid is about $165\,\mathrm{m\,s^{-1}}$. Thus, the Mach number of the outer front of the ring, which is a collapsing wave, is not less than 2.06.

Example 4.2. In figure 18(*g*), the outer radius of the ring pointed out by the white arrow is about 4.1 mm. It takes less than $6.0\,\mu$s to form this ring. Assuming this ring grew from a tiny liquid/vapour drop, the average speed of the outer front of the ring is not less than $683\,\mathrm{m\,s^{-1}}$, yielding the Mach number 4.14.

There are many other smaller rings in the photographs. Since the photograph does not show the time when the rings were initiated, we cannot conclusively estimate the speed of front propagation for these small rings.

The above two examples show that the outer front of the rings of cloud are supersonic. This observation agrees with our conclusion in § 3 that collapsing waves are supersonic.

Remark. An existing conjecture on the reason for the formation of the ring of cloud is that as the incident shock passes a liquid drop or other heavy particles at the window, there is a velocity difference between the drop and the surrounding vapour. This difference causes the formation of vortex rings, visible as the ring of cloud. However, there is no detailed analysis showing this is possible. In particular, why is there cloud inside the vortex rings, and vapour in the centre of the rings? How is it possible that a tiny drop of μm order can cause such a big velocity difference as to make a vortex ring of mm order? How is it possible that an incident shock of Mach number 2.87 can produce a vortex ring that travels perpendicularly to the incident shock at Mach number 4? The mechanism of liquid drops causing a velocity gradient is also present in the open-end shock tube experiments. Why are there no such rings observed in the open-end shock tube experiments? To validate the conjecture, one has to do a detailed analysis and answer these questions. Our explanation answers all the above questions.

The model (3.1) also explains why rings are absent behind the liquefaction shock in the open-end shock tube experiments depicted in figure 4(*b*). The liquefaction wave

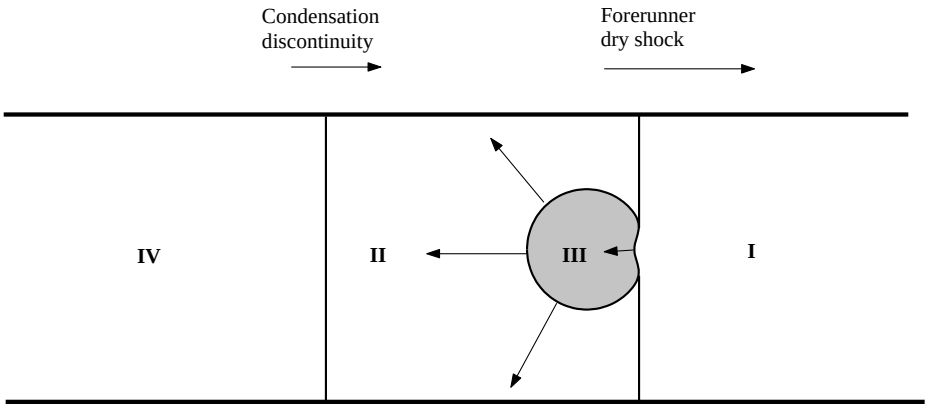

FIGURE 19. Region I is stable vapour, II is metastable vapour. Regions III and IV are filled with liquid/vapour mixture. The thin arrow indicates the motion relative to fluid particles. The open arrow indicates motion of waves relative to Euler coordinate. The front III → II moves faster than the front I → III. Thus, the droplet III cannot evolve into a ring without a wall.

has two parts: first it pushes the pressure of vapour above the equilibrium pressure in region II, then the condensation occurs at the interface IV → II (see figure 19). When the Mach number of the liquefaction shock is high, region II is thin. Since region IV is already filled with liquid/vapour mixture, the only possible place for rings of liquid/vapour mixture to form is in II. Now, the question becomes whether a liquid/vapour mixture droplet in region II can evolve into a ring of liquid/vapour mixture. Since there is no reflection wall, and because the front III → II moves faster than I → III, it is impossible for the front I → III to penetrate region III to form a ring.

Furthermore, figure 19 also suggests a mechanism for the 'button' on the liquefaction shock IV → II observed at the exit of an open-end shock tube in experiments on retrograde fluids, shown in figure 5(*a*). Thompson *et al.* (1986) observed, in figures 20 to 23 of their paper, the transition from smooth to chaotic liquefaction shock fronts with increasing shock Mach numbers. They pointed out a few unusual surface structures during the transition, such as a 'button' at the centre, small-scale surface asperities, and instability of the phase boundaries. Consider the waves IV → II → I in figure 19 at the exit of the open end of the shock tube. The place in region II with the highest pressure is at the central axis of the tube. Then, a liquid/vapour mixture drop is most likely to initiate at the central axis of II. After the initiation of the first liquid/vapour mixture drop, the fronts II → I and I → III in figure 19 move in opposite directions, and the front III → II moves much faster than I → III does. When region II is thin relative to the tube diameter, regions III and IV, both filled with mixture, will quickly merge. This will create a 'button'-like structure at the liquefaction shock front, most likely at its centre. When the incident shock is faster, making the pressure in region II higher, many liquid/vapour mixture drops can appear almost simultaneously. Then the above mechanism leads to the appearance of many small-scale asperities at the liquefaction shock front. Such small-scale surface asperities were observed in experiments by Thompson *et al.* (1986), shown in the photograph figure 22(*d*) in their paper. This raises the question whether the perturbation of liquid/vapour mixture drops lead to the instability of the front IV → II. Answering this question requires a detailed analysis of the stability of the liquefaction travelling wave. We leave it for future investigations.

5. Conclusion

An explanation for the symmetry breaking and the formation of rings of cloud at the endwall of shock tube experiments on retrograde fluids is provided. This explanation is based on the analysis of a prototype model for qualitative studies of liquid/vapour phase transitions in shock tubes proposed by Fan (1998). After the reflection of the incident dry shock, the pressure behind the reflected shock increases to above p_e. Many liquid/vapour droplets appear and grow behind the reflection shock due to this higher pressure, breaking the cylindrical symmetry of the fluid flow. The front of a liquid/vapour drop is shown to evolve into a ring, with the help of the endwall. It is also shown that without the endwall, the front will not evolve into a ring, coinciding with the experimental observations. Furthermore, the surface structures, such as the 'button' at the centre and small-scale surface asperities, of the liquefaction shocks at the exit of an open-end shock tube observed by Thompson *et al.* (1986), are also explained.

The model used in this paper has already been shown in Fan (1998, 2000*b*) to exhibit all the one-dimensional wave patterns listed in Thompson *et al.* (1987). In this paper, two more types of one-dimensional waves, collapsing waves and explosion waves, are numerically demonstrated to exist. The states in front of the collapsing wave and explosion wave are metastable vapour and metastable liquid, respectively. The states behind these waves are liquid/vapour mixture at equilibrium. It is found that these waves are supersonic. Their speeds increase as the ratio μ/γ and $|p_+ - p_e|$ increase. Here p_+ is the pressure in front of the collapsing wave and explosion wave. The outer front of a liquid/vapour ring of cloud is a collapsing wave. Thus, one can estimate the speed of a collapsing wave from photographs of experiments to see whether they are supersonic as predicted by analysis of the model. Such estimation from some photographs from Gulen *et al.* (1994) yields that the Mach numbers of outer fronts of rings considered to range from 2 to 4, as expected.

This research was supported by NSF INT 011513.

REFERENCES

Abraham, F. F. 1974 *Homogeneous Nucleation: The Pretransition Theory of vapour Condensation.* Academic.

Bauschdorff, D. 1975 Carrier gas effects on homogeneous nucleation of water vapour in a shock tube. *Phys. Fluids* **18**, 529–535.

Delale, C. F., Schnerr, G. H. & Zierep, J. 1993*a* Asymptotic solutions of transonic nozzle flows with homogeneous condensation, I, subcritical flows. *Phys Fluids* A **5**, 2969–2981.

Delale, C. F., Schnerr, G. H. & Zierep, J. 1993*b* Asymptotic solutions of transonic nozzle flows with homogeneous condensation, II, supercritical flows. *Phys Fluids* A **5**, 2982–2995.

Dettelff, G., Thompson, P. A., Meier, G. E. A. & Speckmann, H.-D. 1979 An experimental investigation of liquefaction shock wave. *J. Fluid Mech.* **95**, 279–304.

Fan, H.-T. 1993 One-phase Riemann problem and wave interactions in systems of conservation laws of mixed type. *SIAM J. Math. Anal.* **24**, 840–865.

Fan, H.-T. 1998 Travelling waves, Riemann problems and computations of a model of the dynamics of liquid/vapour phase transitions. *J. Diffl Equat.* **150**, 385–437.

Fan, H.-T. 2000*a* Convergence to travelling waves in two model systems related to the dynamics of liquid/vapour phase changes. *J. Diffl Equat.* **168**, 102–128.

Fan, H.-T. 2000*b* On a model of the dynamics of liquid/vapour phase transitions. *SIAM J. Appl. Maths* **60**, 1270–1301.

Fickett, W. & Davis, W. C. 1979 *Detonation.* University of California Press, Berkeley.

Fuchs, N. A. & Sutugin, A. G. 1970 *Highly Dispersed Aerosols*. Ann Arbor Science Publishers, Ann Arbor.

Glass, I. I., Kalra, S. P. & Sisilian, J. P. 1977 Condensation in water vapour in rarefaction waves: III Experimental results. *AIAA J*. **15**, 686.

Gulen, S. C. 1992 A study of shock splitting and liquefaction shocks in fast phase changes in retrograde fluids, Dissertation. Rensselaer Polytechnic Institute.

Gulen, S. C., Thompson, P. A. & Cho, H.-J. 1994 An experimental study of reflected liquefaction shock waves with near critical downstream states in a test fluid of large molar heat capacity. *J. Fluid Mech.* **277**, 163–196.

Homer, J. B. & Hurle, I. R. 1972 Shock tube studies on the decomposition of tetramethyl-lead and the formation of the lead oxide particles. *Proc. R. Soc. Lond*. A **327**, 61.

Jiang, G.-S. & Shu, C. W. 1996 Efficient implementation of weighted ENO schemes. *J. Comput Phys.* **1261**, 202–228.

Kawada, H. & Mori, Y. 1973 A shock tube study of condensation kinetics. *Bull. Japan Soc. Mech. Engrs* **16**, 1053.

Kim, Y.-G. 1987 Shock splitting with phase changes in a liquid-vapour system. PhD Thesis, Rensselaer Polytechnic Institute.

Kluwick, A. & Scheichl, St. 1996 Unsteady transonic nozzle flow of dense gases. *J. Fluid Mech.* **310**, 113–137.

Kotake, S. & Glass, I. I. 1977 Condensation in water vapour in rarefaction waves: II. Heterogeneous nucleation. *AIAA J*. **15**, 215.

Kotake, S. & Glass, I. I. 1981 Flows with nucleation and condensation. *Progr. Aerospace Sci.* **19**, 129–196.

Lee, C. F. 1978 An experimental investigation of the critical supersaturation of five vapours in a shock tube. Dissertation, Yale University.

Oswatitsch, K. 1942 Kondensationserscheinungen in überschalldüsen. *Z. Angew. Math. Mech.* **22**, 1–14.

Oxtoby, D. W. 1992 Homogeneous nucleation:theory and experiment. *J. Phys.: Condens. Matter* **4**, 7627–7650.

Rabie, R. L., Fowles, G. R. & Fickett, W. 1979 The polymorphic detonation. *Phys. Fluids* **22**, 422–435.

Shearer, M. 1986 Nonuniqueness of admissible solutions of Riemann initial value problem for a system of conservation laws of mixed type. *Arch. Rat. Mech. Anal.* **93**, 45–59.

Sisilian, J. P. 1975 Condensation of water vapour with or without a carrier gas in a shock tube. *Univ. of Toronto UTIAS Rep.* 201.

Sisilian, J. P. & Glass, I. I. 1976 Condensation of water vapour in rarefaction waves: I. homogeneous nucleation. *AIAA J*. **14** 1731–1737.

Skripov, V. P. 1974 *Metastable Liquids*, John Wiley & Sons.

Slemrod, M. 1983 Admissibility criterion for propagating phase boundaries in a van der Waals fluid. *Arch. Rat. Mech. Anal.* **81**, 301–315.

Smolders, H. J., Niessen, E. M. J. & van Dongen, M. E. H. 1992 The random choice method applied to non-linear wave propagation in gas-vapour-droplets mixtures. *Comput. Fluids* **21**, 63–75.

Springer, G. S. 1978 Homogeneous nucleation. *Adv. Heat Transfer* **14**, 281–345.

Thompson, P. A., Carofano, G. C. & Kim, Y.-G. 1986 Shock waves and phase changes in a large-heat-capacity fluid emerging from a tube. *J. Fluid Mech.* **166**, 57–92.

Thompson, P. A., Chaves, H., Meier, G. E. A., Kim, Y.-G. & Speckmann, H.-D. 1987 Wave splitting in a fluid of large heat capacity. *J. Fluid Mech.* **185**, 385–414.

Wagner, P. E. 1982 Aerosol growth by condensation. *In Aerosol Microphysics II – Chemical Physics of Microparticles* (ed. W. H. Marlo), ch. 5, pp. 129–178. Springer.

Wegener, P. P. 1969 Gas dynamics of expansion flows with condensation and homogeneous nucleation of water vapour. In *Nonequilibrium Flows* (ed. P. P. Wegener), vol. I, ch. 4, pp. 163–243. Marcel Dekker.

Wegener, P. P. 1975 Nonequilibrium flows with condensation. *Acta. Mech.* **21**, 65–91.

Wegener, P. P. & Lee, C. F. 1983 Condensation by homogeneous nucleation of H_2O, C_6H_6, CCl_4 and CCl_3F in a shock tube. *J. Aerosol. Sci.* **14**, 29–37.

WEGENER, P. P. & LUNDQUIST, G. 1951 Condensation of water vapour in the shock tube below 150 K. *J. Appl. Phys.* **22**, 233.

WEGENER, P. P. & MACK, L. M. 1958 Condensation in supersonic and hypersonic wind tunnels. In *Advances in Applied Mechanics* (ed. H. L. Dryden & T. von Kármán), vol. V, pp. 307–447. Academic Press.

WEGENER, P. P. & WU, B. C. J. 1977 Gas dynamics and homogeneous nucleation, In *Nucleation Phenomena* (ed. A. C. Zettlemoyer), pp. 325–417. Elsevier.

WU, B. J. C. 1977 Analysis of condensation in the centered expansion wave in a shock tube. In *Condensation in High Speed Flows* (ed. A. A. Pouring), pp. 73–82. ASME.